Surface Analysis Studies of Yield Enhancements in Secondary Ion Mass Spectrometry by Polyatomic Projectiles†

Erick R. Fuoco,‡ Greg Gillen,§ Muthu B. J. Wijesundara,‡ William E. Wallace,§ and Luke Hanley*,‡

Department of Chemistry (MC 111), University of Illinois at Chicago, Chicago, Illinois 60607-7061, and Surface and Microanalysis Science Division (MS 8371), National Institute of Standards and Technology, Gaithersburg, Maryland 20899

Received: September 16, 2000; In Final Form: November 14, 2000

In this paper we examine the mechanism of secondary ion yield enhancements previously observed for polyatomic projectiles by measuring the weight loss, volume loss, and surface composition of poly(methyl methacrylate) (PMMA) films sputtered by keV SF_5^+ and Ar^+ projectile ions. The sputter yield—the amount of material removed from the surface by 3.0 keV SF_5^+ projectiles—was found to be 2.2 ± 0.8 higher than for Ar^+ projectiles, measured by weight loss in the PMMA film with a quartz crystal microbalance. This result is consistent with sputter yield measurements reported here using 5.5 keV ions and stylus profilometry. Thus, the $>10\times$ enhancement in secondary ion yield in secondary ion mass spectrometry observed for polyatomic ion projectiles is not attributable to the modest $\sim 2\times$ enhancements observed in the sputter yields for this molecular solid. Surface chemical measurements by X-ray photoelectron spectroscopy also indicated fundamental differences in atomic versus polyatomic sputtering mechanisms at 3.0 keV, but not at 0.7 keV. These results provide a reasonable explanation for the depth profiling capability demonstrated here on PMMA films for 5.5 keV SF_5^+ ions that is not possible with isoenergetic Ar^+ ions.

I. Introduction

Secondary ion mass spectrometry (SIMS) is the most widely used mass spectrometric technique for the surface analysis of molecular solids composed of organic, polymeric, and biomolecular species.[1−5] Enhanced secondary ion yields—the number of sputtered ions produced per projectile ion impact—would improve the sensitivity of SIMS and expand its usage yet further in the surface analysis of molecular solids. Increasing the projectile ion mass and kinetic energy enhances the secondary ion yields due to improved momentum transfer to the surface. Use of polyatomic projectile ions also enhances secondary ion yields when compared to atomic ions of similar or lower mass.[6−12] This polyatomic enhancement also depends on the substrate, with metals showing the smallest effect and molecular solids showing the largest effect. It remains unclear whether this enhancement is due to enhanced desorption, enhanced ionization, or both. In the case of molecular solids, this enhancement might also be due to reduced fragmentation during the desorption/ionization process. In this paper we examine the mechanism of secondary ion yield enhancements by weight loss, volume loss, and surface analysis measurements of poly(methyl methacrylate) (PMMA) films sputtered by keV SF_5^+ and Ar^+ projectile ions.

Many studies have observed enhancements of secondary ion yields in SIMS for SF_5^+ compared with Ar^+ or Xe^+ bombardment of molecular monolayers and solids. These enhancements vary dramatically with sample preparation conditions and both the mass and charge of the secondary ions.[6−9,12,13] For example, 10 keV projectile ion bombardment of arachidic acid Langmuir−Blodgett (LB) layers showed a $5-1000\times$ secondary ion yield enhancement depending on the thickness and composition of the film and the secondary ion identity.[10] Furthermore, monolayer thick samples generally showed little enhancement, especially when compared to the larger enhancements observed for multilayers.[10,11,14] Studies on polymethacrylate LB layers showed similar results for 11 keV projectile ion bombardment, with an enhancement of $14\times$ for the monolayer and $39\times$ for the thickest multilayer examined.[11] Studies on spin-coated PMMA have shown a $7.9-10.8\times$ enhancement, depending on the identity of the fragment ion.[15]

Molecular dynamics simulations have been used to understand the polyatomic enhancement in SIMS. Molecular dynamics simulations studied the effect of projectile ion size on yield by comparing atomic and polyatomic projectiles bombarding single adsorbed molecules on metal and semiconductor surfaces.[16,17] Simulations comparing 0.6 keV Xe^+ versus SF_5^+ sputtering of biphenyl adsorbed on Cu(001) and Si(100) surfaces found the polyatomic projectile enhanced the total yield of desorbed molecules by a factor of 1.2−3.9, depending upon the substrate.[17] This enhancement was found to be due in part to overlapping collision cascades because the probability for overlapping cascades is much higher when two or more atoms are bound together in a polyatomic projectile. Less dense substrates were also found to have higher total desorption yields and larger polyatomic enhancements in these simulations (see below).

Monte Carlo simulations have also been used to examine the polyatomic enhancement effect in SIMS.[18] Simulations on 0.1−1.0 keV Xe^+ and SF_5^+ bombardment of a NH_3/CO bilayer on Ni(111) showed a $2-3\times$ increase in total desorption yield for SF_5^+, in general agreement with adjacent experiments that

† Part of the special issue "John T. Yates, Jr. Festschrift".

* To whom correspondence should be addressed. E-mail: lhanley@uic.edu.
‡ University of Illinois at Chicago.
§ National Institute of Standards and Technology.

10.1021/jp0033317 CCC: $20.00
Published on Web 01/18/2001

measured total sputtering yields (desorption cross-sections) for the same system. The Monte Carlo simulations indicated that the predominant mechanism of polyatomic enhancement was sputtering of adsorbates during backscattering of the S and F atoms off the Ni substrate. This mechanism is reminiscent of that proposed for the larger enhancement off less dense substrates:[17] decomposition of the SF_5^+ projectiles beneath the surface leads to more efficient momentum transfer to and desorption of the molecules at the surface.

Both experiments and simulations have focused mainly on desorption effects to explain the polyatomic enhancement in SIMS. However, experimental results are based upon secondary ion yields that are strongly affected by ionization efficiency.[5] Different yield enhancements have been recently observed for positive versus negative secondary ions emitted from the same samples, clearly indicating a role for ionization effects in the enhancement phenomenon.[12] Unfortunately, molecular dynamics and Monte Carlo simulations typically do not account for ionization effects but rather consider only the total amount of material sputtered, regardless of its charge state. While simulations have directly compared atomic and polyatomic projectile sputtering for isolated adsorbates, monolayers, and bilayers on solid substrates, a similar comparison has not been made on thick layers of molecular solids. One approach to addressing discrepancies between experiments and simulations is the concept of transformation probability, defined as the secondary ion yield per amount of material sputtered.[11] The transformation probability implicitly includes both ionization efficiency and fragmentation of secondary species. There has also been speculation that the chemical nature of the projectile ion might affect the secondary ion yield and that the enhancement for SF_5^+ is due to its high fluorine content. However, at least one study has concluded chemical effects do not explain the enhancement since there was no significant difference between polyatomics that contain fluorine, SF_5^+, versus those without fluorine, $C_7H_7^+$ and $C_{10}H_8^+$.[11]

SIMS is commonly used for depth profiling of inorganic materials,[1] yet ion damage effects have prevented depth profiling of molecular solids. Polyatomic projectiles reduce the decay in molecular secondary ion signal with increasing projectile fluence for some molecular solids, opening up the possibility of depth profiling.[19] Polyatomic projectiles not only increase the secondary ion yields, but also increase the total damage cross-section to an organic substrate.[8,10] However, polyatomic projectiles cannot penetrate through the substrate lattice as easily as atomics, causing this damage to be confined to a shallower region.[7,20] The higher erosion rate and lower penetration depth of polyatomics apparently overcome the higher damage cross-sections to permit depth profiling for at least some molecular solids.

In this paper we investigate the differences between the bombardment of PMMA thick films by two atomic and polyatomic projectile ions, keV Ar^+ and SF_5^+. Sputter yields—the amount of material removed from the surface by SF_5^+ or Ar^+ projectiles—were obtained by weight loss in the PMMA film measured by a quartz crystal microbalance. Sputter rate measurements were also conducted with a magnetic sector SIMS instrument using stylus profilometry. Finally, the surface chemistry following projectile ion impact was examined by X-ray photoelectron spectroscopy. It is shown here that, for PMMA, the $>10\times$ enhancement in secondary ion yield in SIMS observed for polyatomic ion projectiles is not attributable to the modest $\sim 2\times$ enhancement in the sputter yield. The surface chemical measurements also indicate some fundamental differences in atomic versus polyatomic sputtering mechanisms. These results are compared to depth profiling measurements of PMMA by keV Ar^+ and SF_5^+ obtained with the SIMS instrument. Finally, these results are discussed in terms of proposed mechanisms of polyatomic projectile enhancement of secondary ion yields.

II. Experimental Section

PMMA films were prepared by spin-casting a solution of 2% PMMA (Aldrich, average $M_w \approx 350\,000$) dissolved in *o*-xylene or toluene solvent. The samples for SIMS and X-ray photoelectron spectroscopy (XPS) were spin-cast at 2000 rpm onto 3 in. diameter Si(111) wafers. Ellipsometry showed the films to be 50−60 nm thick. Samples for quartz crystal microbalance (QCM) analysis were prepared by spin-casting the solution onto the gold sensor crystals using a home-built spin coater. The QCM samples were coated as thick as possible while maintaining a stable frequency in vacuum; however, their absolute thicknesses were not determined. The samples spin-cast onto Si were expected to be smooth on a nanometer scale, while the samples spin-cast onto Au were rough on a micrometer scale, following the rough Au QCM crystal surface morphology. These differences in roughness and thickness between the two types of PMMA samples should be taken into account when the data from the two experiments are compared.

SIMS experiments on the spin-cast PMMA films were conducted with a magnetic SIMS instrument (Cameca IMS 4F) using bombardment with either an Ar^+ or SF_5^+ projectile ion beam from a custom-built triplasmatron ion source.[21] The projectile ion beam impact energy was 5.5 keV with an impact angle of 42° with respect to the surface normal. A focused projectile ion beam of 0.2−1.0 nA was rastered over an area of 250 μm × 250 μm as a function of increasing time. Sputter yield measurements were made by measuring the depth of erosion as a function of projectile ion dose. Depth measurements were made with a surface profilometer (Tencor Alpha Step 200). Depth profiles of the PMMA films were conducted while monitoring positive secondary ions. The rapid increase in the silicon substrate ion signal was used to indicate that the film was completely eroded. Measurements were not performed with Xe^+ projectiles due to the difficulty of focusing the different Xe^+ isotopes into the same spot on the surface, a requirement for accurate measurements of depth profiles.

The instrumentation used for ion bombardment[18] and XPS analysis[22] has been described previously. Briefly, the system consists of a differentially pumped ion source attached to a preparation chamber which is kept at a base pressure of $\sim 1 \times 10^{-8}$ Torr. The 0.7 keV ions were formed in an 80 eV electron impact ion source from Ar or SF_6 gas (AGA), accelerated to ~1000 eV, mass separated by a Wien filter, bent 3° to remove fast neutrals, decelerated, refocused, and guided by a series of lenses to impact the substrate at a normal angle. Typical currents were 15−30 nA for SF_5^+ and 50−70 nA for Ar^+ over a 5 mm spot. A change in the ion source electronic configuration from that previously described was used to form >1 keV ions. The 3 keV ions were formed in a similar fashion except that they were not decelerated prior to impact. Typical currents were 14−20 nA for SF_5^+ and 35−45 nA for Ar^+. For QCM analysis, the current was increased to 100−130 nA for both ions and the ion beam was centered on the QCM probe opening. The preparation chamber pressure rose to $\sim 8 \times 10^{-8}$ Torr during bombardment.

XPS analysis was done with a high-resolution monochromatic Al Kα X-ray source (15 keV, 25 mA emission current, VSW Rowland circle monochromator) and a 150 mm concentric

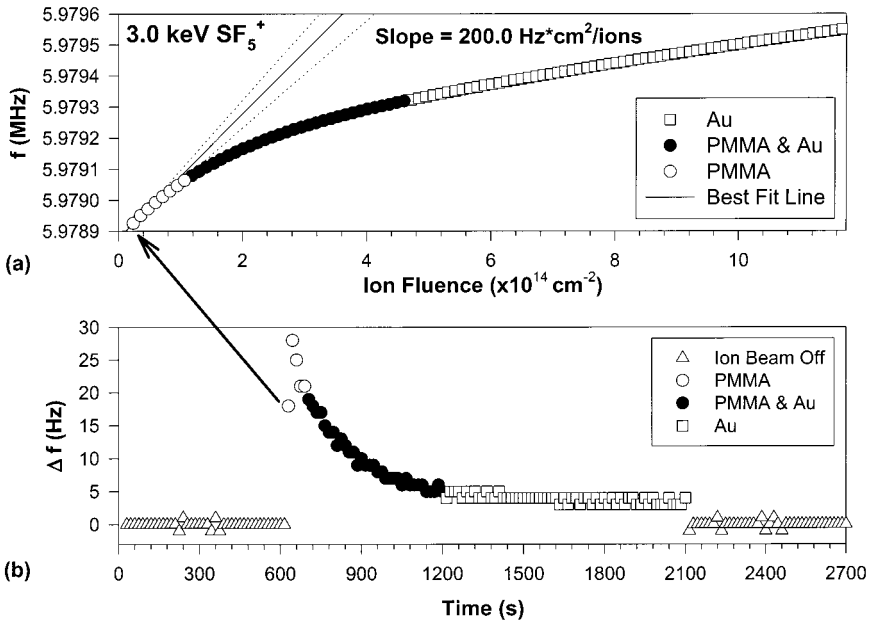

Figure 1. (a) QCM frequency response versus fluence for 3 keV SF_5^+ bombarding a PMMA thin film on a gold sensor crystal at normal incident angle. (b) Change in frequency between successive data points.

hemispherical analyzer with a multichannel detector (VSW Class 150). The angle of photoemission was normal to the surface. The pass energy was kept at 22 eV for all spectra. All XP spectra were referenced to the aliphatic C(1s) core level photoemission peak at 285.0 eV. Peak areas were found using commercial software (Spectra, VSW). Elemental percentages were determined from the peak areas of each component with the aid of elemental sensitivity factors[23] and the transmission function for the analyzer (VSW). The base pressure of the XPS chamber was $\sim 2 \times 10^{-9}$ Torr.

The QCM measurements were performed using a modified 6 MHz probe (Sycon). The output frequency was read using a Sycon STM 100/MF thickness monitor. The probe was attached to the sample manipulator to achieve the same position as samples in XPS. The water lines were disconnected to allow for its translation from the load lock into the preparation chamber. A copper braid was attached to the probe on one end and to a dewar on the other end. The copper braid kept an equilibrium temperature near 300 K on the probe by a flow of He gas through the dewar. The frequency output of the STM 100/MF was read every 15 s by customized software (Lab View, National Instruments) via an RS-232 port.

III. Results and Discussion Section

A. Sputter Yield Measurements by a Quartz Crystal Microbalance. Measurements for the total sputter yield were acquired using a QCM. It has been shown that the QCM can be used to study the etch rates of films by low-energy ion beams.[24] The frequency change, Δf (Hz), is linearly dependent on the mass change, Δm (ng/cm^2), as described by the following equation:[25]

$$\Delta m = D_\infty \Delta f$$

where D_∞ is a constant for the crystal/film combination which will cancel out in the measurements presented here. The maximum Δf observed in these experiments was <1 kHz, far less than the 120 kHz maximum allowable Δf for which the above equation remains valid.[24] Once the Au crystal had been placed in a vacuum and its temperature stabilized, the drift in Δf was <1 Hz/15 min. The QCM operation was verified by observation of a linear response in Δf for a bare Au sensor crystal bombarded with 3 keV SF_5^+ and Ar^+ (data not shown but similar to data in Figure 1a at ion fluences above 4×10^{14} cm^{-2}).

Figure 1a displays the QCM frequency response versus SF_5^+ fluence for bombardment of PMMA. Similar data were collected for Ar^+ and display a similar pattern of frequency response (data not shown). Figure 1a displays an initial sharp increase in frequency with the initial sputtering and a linear increase at higher fluences. Figure 1b graphs these same data as Δf between adjacent data points, leading to the observation of four distinct regions in this curve. The arrow indicates matching points between the two parts of Figure 1. The first region of Figure 1b shows $\Delta f = 0$ Hz and corresponds to when the ion beam is off. The second region shows the largest Δf and corresponds to the sputtering of pure PMMA: this is the region to be analyzed. The third region is where Δf decreases as PMMA and Au sputtering overlap. The fourth region is a constant Δf, corresponding to sputtering of the underlying gold for SF_5^+ or a carbon-rich material for Ar^+. Ar^+ does not appear to have sputtered completely through the PMMA in the time allotted for the experiment, but rather reaches a steady Δf. Visual examination appears to support these results: the region of PMMA bombarded by SF_5^+ appears similar to clean gold, whereas the area bombarded by Ar^+ turns black.

The slope of the initial linear region (labeled "PMMA" in Figure 1) is determined by assuming that only PMMA is being sputtered in this region. The slope of the Δf versus 3 keV SF_5^+ ion fluence line is $(1.9 \pm 0.5) \times 10^{-12}$ (Hz·cm^2)/ion, whereas the slope from the 3 keV Ar^+ line is $(0.9 \pm 0.2) \times 10^{-12}$ (Hz·cm^2)/ion. The sputter yield for 3.0 keV SF_5^+ projectiles is enhanced 2.2 ± 0.8 times compared with Ar^+ projectiles, determined by taking the ratios of the two slopes. The QCM was not sensitive enough to make a similar measurement with 0.7 keV ions.

B. Sputter Rate Measurements by Stylus Profilometry. Absolute sputter rates were also measured by using the projectile ion beam to dig a hole in the PMMA film as a function of ion fluence. This gave a series of craters of increasing depth which

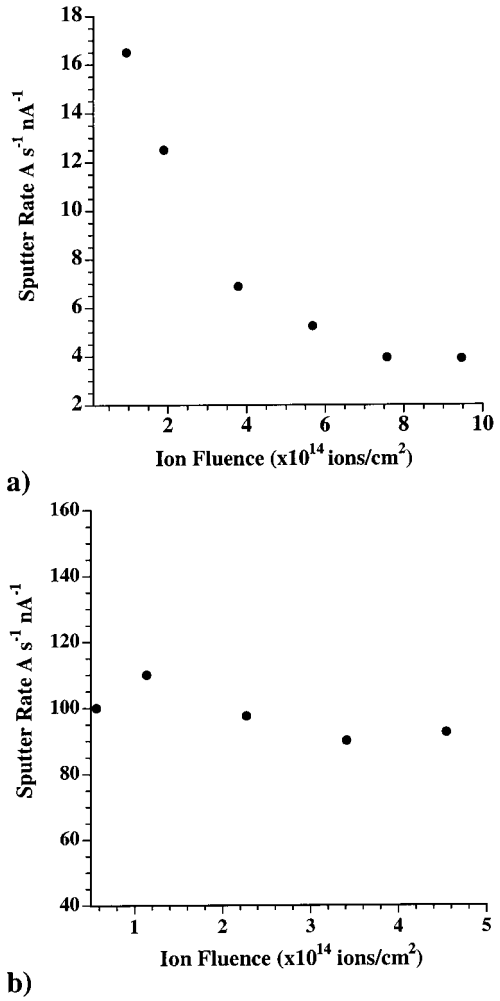

Figure 2. Sputter rate measurements incident on a PMMA thin film on Si by 5.5 keV (a) Ar^+ and (b) SF_5^+ projectiles via stylus profilometry, recorded at 42° incident angle.

were then measured with a profilometer. From the ion fluence and crater size, the erosion yield or sputter rate of the film was obtained. Under the conditions used to measure these sputter rates, it was typically found that the characteristic ions of PMMA give a 10−30× higher secondary ion signal via bombardment with SF_5^+ vs Ar^+ (secondary ion data not shown).

Figure 2 displays the sputter rate of the polymer film as a function of projectile ion dose for bombardment with 5.5 keV Ar^+ and SF_5^+ projectile ions at 42° off the surface normal. SF_5^+ has a higher sputter rate than Ar^+ at all fluences, with a steady-state enhancement of 20×. However, if the curve for Ar^+ is extrapolated to the ideal static SIMS region, the sputter rate for SF_5^+ enhancement reduces to 2−3×. This value is consistent with that obtained from the QCM measurement, despite the latter's use of a low projectile ion energy (3 keV) and normal incident angle.

The QCM measurements with 3 keV SF_5^+ ions sputtered through the PMMA film on the Au sensor crystal (Figure 1). By contrast, the 5.5 keV SF_5^+ ion craters measured in PMMA by stylus profilometry did not indicate a complete sputtering through the PMMA film on Si. This difference is due to the higher SF_5^+ ion currents used in the QCM experiments and the differences in PMMA film morphology and thickness (see the Experimental Section).

C. Change in Surface Concentration after Bombardment by 3 keV Projectile Ions. Examination of the surface chemistry induced by ion bombardment provides further information on

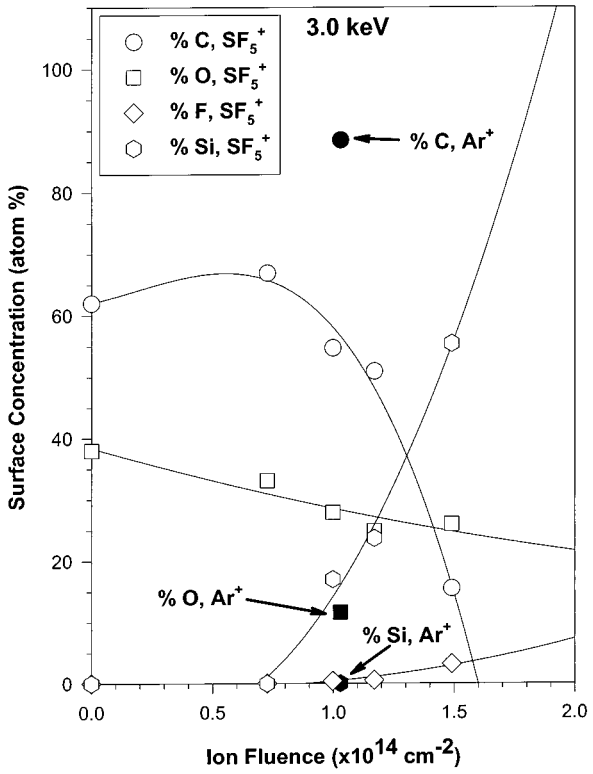

Figure 3. Atomic surface concentration recorded by monochromatic XPS versus ion fluence for 3 keV SF_5^+ projectiles incident on a PMMA thin film on Si. Data for one ion fluence also shown for 3 keV Ar^+ projectiles.

the mechanism for polyatomic enhancement in secondary ion yields. Clear differences in surface chemistry are shown by the survey XPS for PMMA before and after sputtering with 3 keV SF_5^+ and Ar^+. The XP spectra were analyzed to generate Figure 3, which displays the elemental composition as a function of 3 keV SF_5^+ ion fluence, along with the composition for a single 3 keV Ar^+ point. For 3 keV SF_5^+ bombardment, the carbon-to-oxygen ratio (C/O) is constant at ∼1.8 up to a fluence of $\sim 1.0 \times 10^{14}$ ions/cm^2. This indicates that the elemental composition of the PMMA film remains relatively constant until the film is sputtered through, the latter event revealed by the appearance of a Si substrate signal. By contrast, the C/O from 3 keV Ar^+ is ∼7.6 and indicates formation of a carbon-rich material. Previous experiments on the bombardment of PMMA by 5 keV Ar^+ showed the same conversion to a carbon-rich material.[26] It was similarly observed that 10 keV Ar^+ and Xe^+ converted a polystyrene film into a carbon-black-like material.[27]

For 3 keV SF_5^+ bombardment of PMMA at fluences above 1.0×10^{14} ions/cm^2, it is observed here that much of the oxygen remaining is actually due to SiO_2 on the uncovered Si substrate, a fact supported by the simultaneous rise in Si composition (see Figure 3). By contrast, 3 keV Ar^+ bombardment displays no silicon content at 1.0×10^{14} ions/cm^2. The fluence threshold for silicon exposure by SF_5^+ is 7×10^{13} ions/cm^2, where the threshold is defined as the point where the upper ∼8 nm of the substrate reaches a composition of a few atomic percent of silicon. Fluorine also appears on the surface at approximately the same SF_5^+ ion fluences at which silicon is observed to appear. No implanted Ar or S were detected by XPS following sputtering with 3 keV Ar^+ or SF_5^+.

Further information on the chemical composition of the PMMA film can be obtained by examination of the C(1s) core level spectra following ion bombardment. Figure 4 displays the C(1s) XPS peak for native and 3 keV ion modified PMMA

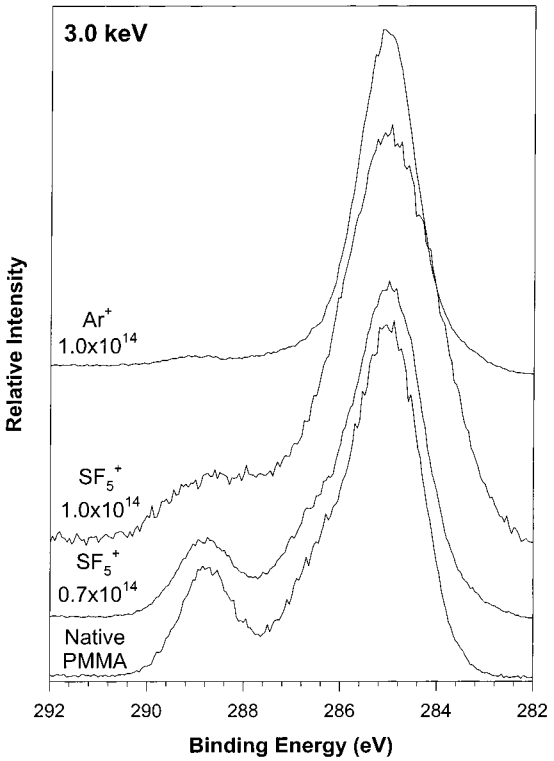

Figure 4. Comparison of the C(1s) core level XPS peak of PMMA bombarded by increasing fluences of 3 keV SF_5^+. Also shown is Ar^+-bombarded PMMA at a fluence of 1.0×10^{14} ions/cm^2.

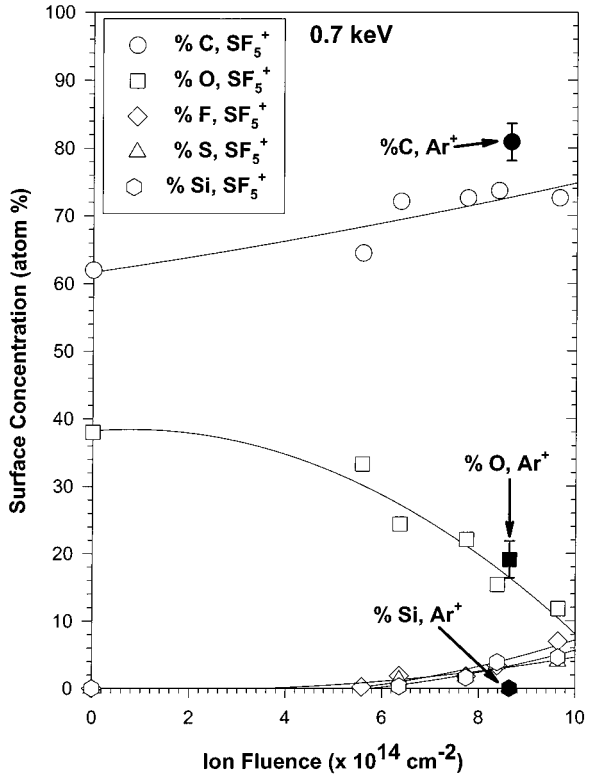

Figure 5. Atomic surface concentration versus fluence for 0.7 keV SF_5^+ incident on a PMMA thin film on Si, from XPS. Data for one fluence also shown for 0.7 keV Ar^+ projectiles.

and indicates a change in the carbon chemical environment. The C(1s) peak has been deconvoluted into three components in Table 1, which lists both the absolute and normalized percentages (in parentheses). The largest component is the aliphatic carbon peak at a binding energy of 285.0 eV. The methoxylic carbon peak occurs at 286.5 eV, and the carboxylic carbon peak occurs at 288.9 eV.[26] A comparison at the same fluence between SF_5^+ and Ar^+ shows that Ar^+ decomposes the carboxylic component more rapidly than does SF_5^+ (Table 1). This confirms that the surface is becoming a highly aliphatic carbon surface—like carbon black—upon 3 keV Ar^+ bombardment. However, Table 1 indicates that less drastic chemical changes are also induced in the PMMA film by 3 keV SF_5^+ bombardment. These chemical changes are also indicated by broadening of the C(1s) peak components following 3 keV SF_5^+ bombardment (see Figure 4).

D. Change in Surface Concentration after Bombardment by 0.7 keV Projectile Ions. The effect of 0.7 keV ion bombardment on the PMMA film chemistry was also examined by XPS. Figure 5 displays a graph of the atomic surface concentration versus fluence for SF_5^+, indicating a different trend than observed above for 3 keV ions. The C/O ratio increases continually from ~2 at 6×10^{14} SF_5^+ ions/cm^2 to ~6 near 10^{15} SF_5^+ ions/cm^2. This increase in C/O is indicative of a gradual conversion of the PMMA surface to a carbon-rich material by 0.7 keV SF_5^+. The fluence threshold for Si exposure is now 5×10^{14} ions/cm^2. Sulfur and fluorine are seen on the surface near the same fluence that silicon is seen. Comparing Ar^+ and SF_5^+ at $\sim 8.5 \times 10^{14}$ ions/cm^2 displays a similar C/O of ~4.4, indicating similar composition following ion bombardment. A closer investigation of the C(1s) peak shows that both projectile ions decompose the carboxylic component with respect to the aliphatic component (Table 1), with both C(1s) peaks displaying almost identical shapes and relative areas. Both 0.7 keV Ar^+ and SF_5^+ appear to be converting the PMMA surface into a carbon-rich material. However, the different C/O ratios and C(1s) component ratios indicate that the carbon-rich material formed by the 0.7 keV ions is not identical to either the carbon-rich material formed by 3 keV Ar^+ or the chemically modified PMMA formed by 3 keV SF_5^+ (although closer to the former).

The XPS results in Figure 5 and Table 1 indicate that both 0.7 keV ions are mechanistically similar with regard to sputtering and different from either 3 keV ion (although apparently closer to 3 keV Ar^+). In a study of SF_5^+ and Xe^+ bombardment of PMMA LB layers, the secondary ion yield of Xe^+ was higher than SF_5^+ for energies <1 keV.[11] These previous results were explained by a low energy per atom of ~150 eV for SF_5^+, which was near the threshold for sputtering. Other work has argued that while less fragmentation is observed for low-energy and high-mass atomic projectiles, polyatomics cause less fragmentation than isobaric atomics.[28] This work

TABLE 1: Deconvolution of the C(1s) Core Level Peak of a Native and Ion-Bombarded PMMA Thin Film on Si into Absolute and Normalized (in Parentheses) Component Percentages

projectile ion and energy	fluence ($\times 10^{14}$ ions/cm^2)	aliphatic carbon (%)	methoxylic carbon (%)	carboxylic carbon (%)
native PMMA	0.0	61.3 (100)	24.2 (39)	14.5 (24)
3.0 keV SF_5^+	1.1 ± 0.1	81.5 ± 4.7 (100)	10.3 ± 4.6 (13 ± 6)	8.3 ± 0.1 (11 ± 0.7)
3.0 keV Ar^+	1.0	93.4 ±1.0 (100)	4.5 ± 0.7 (5 ± 0.5)	2.2 ± 0.4 (2 ± 0.3)
0.7 keV SF_5^+	9.1 ± 0.7	83.3 ±0.4 (100)	11.5 ± 0.1 (14)	5.3 ± 0.5 (7 ± 0.7)
0.7 keV Ar^+	8.6 ± 0.04	81.0 ± 0.8 (100)	14.1 ± 0.9 (17 ± 2)	4.8 ± 1.3 (6 ± 2)

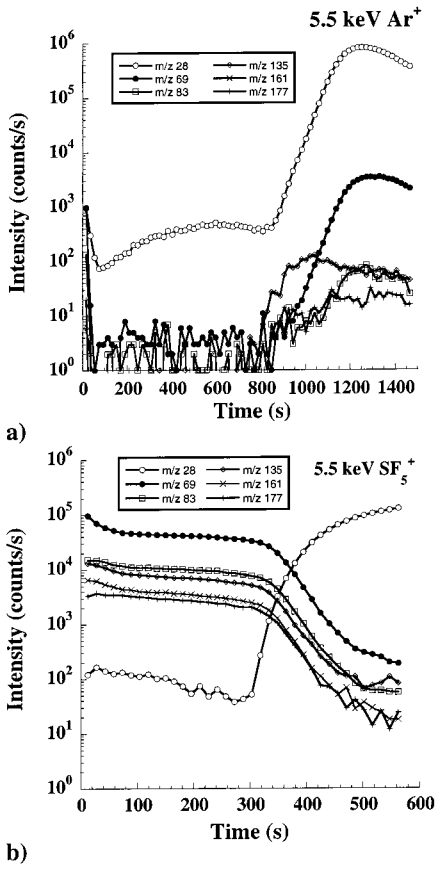

Figure 6. Molecular depth profiling of a PMMA thin film on Si by 5.5 keV (a) Ar^+ and (b) SF_5^+ projectiles, recorded by measuring various secondary ions at 5.5 keV projectile energy and 42° incident angle.

further argued that fragmentation induced by polyatomic projectiles decreased with increasing energy. Both these points are consistent with the chemical transformation of PMMA by 0.7 keV SF_5^+ into a material approaching carbon black, but the maintenance of a significant portion of the PMMA structure by 3 keV SF_5^+.

E. Molecular Depth Profiling of PMMA. Figure 6 plots the intensity of several secondary fragment ions of PMMA versus time for 5.5 keV ion bombardment at 42° off the surface normal. A dramatic difference in behavior is observed for the two projectile ions in the sputtering time dependence of the secondary ion signals. For SF_5^+ projectiles, the intensity of the different fragments stays constant after the initial sputtering, until the film is sputtered down to the underlying Si. The film composition sampled by SIMS does not change during the sputtering process, implying that SF_5^+ projectiles can be used for depth profiling of PMMA films. The surface composition appears to change during Ar^+ bombardment (as shown by the XPS data), precluding the use of Ar^+ for depth profiling of PMMA. Another advantage of SF_5^+ over Ar^+ projectiles for depth profiling is the shallower penetration depth, as indicated by the lower overall Si signal (*m*/*z* 28) appearing after long exposure times. Note that the Si^+ rises sooner from SF_5^+ than from Ar^+ only due to the use of ~5× higher Ar^+ ion currents. The low *m*/*z* 28 signals at lower times from both projectile ions are likely due to CO^+ formed from PMMA decomposition, but may also result from Si^+ emitted from defects in the PMMA film.

It should also be noted in Figure 6 that the SF_5^+ projectiles produce far higher secondary ion signals of the higher mass ions (*m*/*z* 69−177) than does Ar^+, especially when compared at lower ion fluences (time). This is an example of the enhancement in secondary ion yield for the polyatomic projectile.

IV. Conclusions

QCM and profilometry data show a 2−3× enhancement in the sputter yield for 3 keV SF_5^+ bombardment of PMMA when compared to isoenergetic Ar^+. The enhancement is smaller than the 10−30× secondary ion yield enhancement typical for this system. It follows that, for at least PMMA films, the polyatomic enhancement in secondary ion yields cannot be explained solely by an increase in the sputter yield. Previous measurements found monolayer thick samples generally showed little enhancement in secondary ion yields, especially when compared to the larger enhancements observed for multilayers.[10,11,14] However, the results presented here show only small enhancements in total sputter yields from thick PMMA samples, in agreement with our previous results for monolayer systems.[18] It follows that, to establish a complete mechanism for the polyatomic enhancement, ionization and/or fragmentation of the secondary species must also be considered to account for the difference between the total sputter yield and the secondary ion yield.[11] This argument is consistent with experiments that found different enhancements in positive vs negative[12] and low- vs high-mass secondary ion yields from the same sample.[7,12]

Surface analysis found that 3 keV SF_5^+ only slightly modifies the chemical composition of the PMMA film that remains behind after ion bombardment, but 3 keV Ar^+ induces a dramatic chemical conversion of the film into a carbon-rich material. At 0.7 keV, both projectile ions induce similar chemical transformations of the film that are closer, but not identical to, that induced by 3 keV Ar^+. These surface analysis results indicate that different sputtering mechanisms occur for atomic versus polyatomic projectiles at 3 keV. It follows that the enhanced secondary ion yields for polyatomic enhancements may be related to these different sputtering mechanisms. Both the total sputter yield and surface analysis results are consistent with the general notion of a cooperative collision cascade model predicted to enhance secondary ion yields.[17] In particular, a SF_5^+-induced cooperative collision cascade might lead to desorption of intact PMMA-derived ions and neutrals with minimal decomposition of the remaining PMMA on the surface. However, the similarity of the sputtering mechanism at 0.7 keV bombardment—implied by the surface analysis results—is not consistent with the simulations performed at similar energies.[17] It is unclear whether this inconsistency is due to differences in the targets (thick films versus submonolayers), the atomic projectiles (Ar^+ vs Xe^+), or more fundamental reasons.

The surface analysis also provides explanations for both the depth profiling capability and the constant sputter rate with ion fluence observed for PMMA films by 5.5 keV SF_5^+ projectile ions. The SF_5^+ ions may efficiently sputter away PMMA while simultaneously uncovering fresh PMMA for subsequent sputtering events. This mechanism assumes that the volume of the damage region induced by the polyatomic projectile is similar to or smaller than the sputtered volume. By contrast, 5.5 keV Ar^+ ions show a decrease in sputter rate with ion fluence and do not allow depth profiling of PMMA. This is explained by the Ar^+ ions damaging a much deeper volume and inducing a more dramatic chemical transformation within that volume of PMMA. Therefore, subsequent sputtering events sample not native PMMA, but the modified carbon-rich material. These arguments are in agreement with previous comparisons of atomic versus polyatomic ion modification and sputtering of surfaces.[7,18,20]

The similarity of the modification of PMMA by 0.7 keV Ar^+ and SF_5^+ is consistent with the absence of a polyatomic projectile enhancement for organic multilayers with <1 keV projectile ions.[11]

Acknowledgment. This work was funded by the National Science Foundation (Grants CHE-9457709 and CHE-9986226) and the National Institute for Standards and Technology.

References and Notes

(1) Benninghoven, A.; Rudenauer, F. G.; Werner, H. W. *Secondary Ion Mass Spectrometry: Basic Concepts, Instrumental Aspects, Applications, and Trends*; John Wiley & Sons: New York, 1987; Vol. 86.

(2) Benninghoven, A. *Angew. Chem., Int. Ed. Engl.* **1994**, *33*, 1023−1043.

(3) Bertrand, P.; Weng, L. T. *Mikrochim. Acta* **1996**, Suppl. 13, 167−182.

(4) Briggs, D. *Surface Analysis of Polymers by XPS and Static SIMS*; Cambridge University Press: New York, 1998.

(5) Hanley, L.; Kornienko, O.; Ada, E. T.; Fuoco, E.; Trevor, J. L. *J. Mass Spectrom.* **1999**, *34*, 705−723.

(6) Appelhans, A. D.; Delmore, J. E. *Anal. Chem.* **1989**, *61*, 1087−1093.

(7) Le Beyec, Y. *Int. J. Mass Spectrom. Ion Processes* **1998**, *174*, 101−117.

(8) Groenewold, G. S.; Gianotto, A. K.; Olson, J. E.; Appelhans, A. D.; Ingram, J. C.; Delmore, J. E.; Shaw, A. D. *Int. J. Mass Spectrom. Ion Processes* **1998**, *174*, 129−142.

(9) Harris, R. D.; Van Stipdonk, M. J.; Schweikert, E. A. *Int. J. Mass Spectrom. Ion Processes* **1998**, *174*, 167−177.

(10) Stapel, D.; Brox, O.; Benninghoven, A. *Appl. Surf. Sci.* **1999**, *140*, 156−167.

(11) Stapel, D.; Thiemann, M.; Benninghoven, A. *Appl. Surf. Sci.* **2000**, *158*, 362−374.

(12) Wittmaack, K.; Szymczak, W.; Hoheisel, G.; Tuszynski, W. *J. Am. Soc. Mass Spectrom.* **2000**, *11*, 553−563.

(13) Hand, O. W.; Majumdar, T. K.; Cooks, R. G. *Int. J. Mass Spectrom. Ion Processes* **1990**, *97*, 35−45.

(14) Harris, R. D.; Baker, W. S.; Van Stipdonk, M. J.; Crooks, R. M.; Schweikert, E. A. *Rapid Commun. Mass Spectrom.* **1999**, *13*, 1374−1380.

(15) Kotter, F.; Benninghoven, A. *Appl. Surf. Sci.* **1998**, *133*, 47−57.

(16) Zaric, R.; Pearson, B.; Krantzman, K. D.; Garrison, B. J. *Int. J. Mass Spectrom. Ion Processes* **1998**, *174*, 155−166.

(17) Townes, J. A.; White, A. K.; Wiggins, E. N.; Krantzman, K. D.; Garrison, B. J.; Winograd, N. *J. Phys. Chem. A* **1999**, *24*, 4587−4589.

(18) Ada, E. T.; Hanley, L. *Int. J. Mass Spectrom. Ion Processes* **1998**, *174*, 231−244.

(19) Gillen, G.; Roberson, S. *Rapid Commun. Mass Spectrom.* **1998**, *12*, 1303−1312.

(20) Hanley, L.; Sinnott, S. B. *Surf. Sci.*, submitted for publication.

(21) Gillen, G.; King, L.; Chmara, F. *J. Vac. Sci. Technol., A* **1999**, *17*, 845−852.

(22) Wijesundara, M. B. J.; Ji, Y.; Ni, B.; Sinnott, S. B.; Hanley, L. *J. Appl. Phys.* **2000**, *88*, 5004−5016.

(23) Scofield, J. H. *J. Electron Spectrosc. Relat. Phenom.* **1976**, *8*, 129−137.

(24) Doemling, M. F.; Lin, B.; Rueger, N. R.; Oehrlein, G. S.; Haring, R. A.; Lee, Y. H. *J. Vac. Sci. Technol., A* **2000**, *18*, 232.

(25) Sauerbrey, G. *Z. Phys. Chem. (Munich)* **1959**, *155*, 206.

(26) Pignataro, B.; Fragala, M. E.; Puglisi, O. *Nucl. Instrum. Methods Phys. Res., B* **1997**, *131*, 141−148.

(27) Netcheva, S.; Bertrand, P. *Nucl. Instrum. Methods Phys. Res., B* **1999**, *151*, 129−134.

(28) Gilmore, I. S.; Seah, M. P. *Appl. Surf. Sci.* **2000**, *161*, 465−480.